THE JOURNAL OF PHYSICAL CHEMISTRY B

Article

pubs.acs.org/JPCB

Scaling Laws and Ionic Current Inversion in Polyelectrolyte-Grafted Nanochannels

Guang Chen and Siddhartha Das*

Department of Mechanical Engineering, University of Maryland, College Park, Maryland 20742, United States

ABSTRACT: Polyelectrolyte (PE) grafting renders incredible "smartness" to nanochannels, making it capable of applications such as ion manipulation and selection, fabrication of nanoionic diodes, flow control, and so on. In this paper, we provide scaling laws that describe the dominant factors dictating the functioning of such PE-grafted nanochannels. Through these scaling calculations, we identity the phase space for the grafting density (σ) and the polymer size (N) that simultaneously ensures that the grafted PE molecules attain a brush-like configuration and the brush height is smaller than the nanochannel half height. More importantly, we quantify in this phase space the conditions that allow decoupling of the PE electrostatic effects from the PE entropic (elastic) and the excluded volume effects. This decoupled regime is characterized by the fact that the brush height is independent of the PE electrostatic effects. In this decoupled regime, we next calculate the nanochannel ionic current for cases where the PE charge densities depend on pH (or pOH). Our results demonstrate highly interesting current inversion phenomenon originating from the triggering of "co-ion-dominated" ionic current.

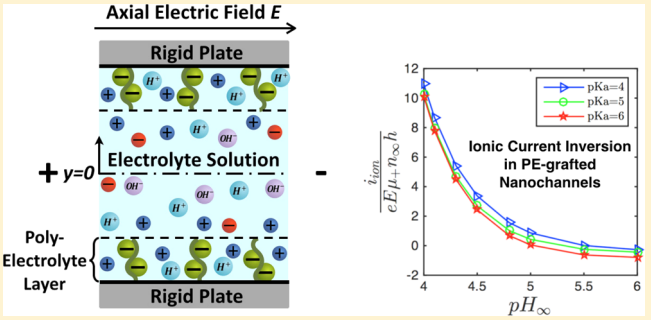

INTRODUCTION

Grafting nanochannels with polyelectrolyte (PE) layers has emerged as a novel technique for a large number of applications such as ion sensing, manipulation, and rectification,[1−4] fabrication of nanofluidic diodes,[5,6] sensing and detection of biomolecules,[4,7,8] valving of liquid transport,[9] designing novel nanoscale energy applications,[10,11] and many more. Motivated by these widespread applications of PE-grafted nanochannels (often denoted as "soft" nanochannels), there have been sustained efforts to model the ion and liquid transport in such nanochannels,[10,12−19] involving appropriate descriptions of the thermodynamics, configuration, and electrostatics of the PE layer.[12,20−23] It is well known that the equilibrium of a grafted PE layer is dictated by the balance of the elastic, volume exclusion, and the electrostatic effects. Although a full-scale model that accounts for all of these effects simultaneously has already been proposed,[20,21] it is inadequate to account for the case of reactive PE systems. To be more specific, for cases where the PE charge density depends on pH, the model becomes inappropriate because it invariably describes the hydrogen ion concentration within the PE layer through Boltzmann distribution;[21] in our recent studies,[12,13] we have demonstrated that such a consideration invariably leads to physically inconsistent hydrogen ion concentration distribution at the PE-layer-surrounding-electrolyte interface. Under these circumstances, it will be immensely useful to know the conditions where one can decouple the PE electrostatic effects from the PE entropic (elastic) and the excluded volume effects. Such decoupling ensures that the PE layer thickness is independent of the PE electrostatic effects, which, in turn, allows a substantially more convenient modeling of the reactive PE-grafted nanochannel systems, thereby shedding light on a large number of unexplained facets associated with ion and liquid transport in PE-grafted nanochannels. It is worthwhile to mention here that there is a large volume of studies that describes the electrostatics and the electrokinetics of a grafted PE layer, assuming the layer to be of constant thickness (see the review articles[24−28] and the references therein). Therefore, all of these studies implicitly assume that the calculations are performed in the decoupled regime, where the PE thickness is independent of the electrostatic effects stemming from the PE charge.

The present study is divided into two parts. In the first part we provide scaling laws for PE-grafted nanochannels. For a given type of PE−solvent−substrate combination, the grafting is dictated by the grafting density σ (this implies there are σ number of PE chains grafted per unit area of the surface) and the PE size N (N is the number of monomers in the PE chain). Our scaling calculations help us to identify the $\sigma-N$ phase space that simultaneously ensure two conditions: (a) the grafted PE molecules attain brush-like configuration and (b) the height of the PE brush is less than the nanochannel half height. This second condition is necessary to ensure that one does not need to consider effects arising from overlap of PE brushes from the two nanochannel walls.[29,30] More importantly, we identify the conditions where, within this $\sigma-N$ phase plot, we can decouple the PE electrostatic effects from the PE entropic and excluded volume effects. This condition is a sole

Received: July 23, 2015
Revised: September 1, 2015

DOI: 10.1021/acs.jpcb.5b07167
J. Phys. Chem. B XXXX, XXX, XXX−XXX

function of σ. We call this σ as the critical grafting density σ_c. We show that $\sigma_c \approx 1/(at)$ (a is the Kuhn length and t is the thickness of the PE molecule), and such decoupling is possible for $\sigma \ll \sigma_c$ or $\sigma \gg \sigma_c$. Because $\sigma \approx l^{-2}$ (where l is the separation between two adjacent grafted PE molecules), the above relation expresses the decoupling condition in terms of the distance of separation l. Finally, we provide actual examples of this $\sigma-N$ phase plot as well as the corresponding σ_c considering poly(acrylic acid) (PAA) and DNA as grafting PE chains.

In the second part of the study, we compute the ionic current induced in the presence of an externally applied axial electric field in such PE-grafted nanochannels in the decoupled regime, that is, where the PE layer thickness is independent of the PE electrostatic effects. Of course, the electrostatic effects are triggered by the PE charges; we consider the case of pH- (or pOH-) dependent PE charge for a negatively (or positively) charged PE layer. We obtain the most nonintuitive result where for certain combination of parameters (i.e., combinations of surrounding pH (or pOH) and pK_a (or pK_b) values of the dissociating acid (basic) group that produces the PE charge for negative (positive) PE layer) the ionic current becomes co-ion dominated; in other words, despite the electrostatic potential being negative (or positive) for a negative (or a positive) PE layer, we get a negative (or a positive) ionic current. We describe this phenomenon as ionic current inversion because the ionic current has a sign opposite to what is expected, given the sign of the counterions. This is the second key finding of this paper. Please note that this inversion is different from charge inversion (CI) and the inversion of streaming current typically employed to quantify this CI.[31,32] In CI, which is typically caused by the presence of multivalent counterions[33−35] or finite sized monovalent co-ions and counterions,[36] the electrostatic potential in the vicinity of the charged wall shows a sign opposite to that of the bare charge; this inversion is quantified by measuring the corresponding inversion of the streaming current triggered by the downstream advection of mobile electrolyte ions within the electric double layer (or EDL) in the presence of a background pressure-driven transport.[37−44] Quantifying ionic current is central to a number of applications of nanochannels with and without PE grafting; some of these applications are sensing and detecting biomolecules, devising nanofluidic diodes and rectifiers, and so on. For all of these applications, it is paramount to know the base state current. For example, the knowledge of the change of the base state current or the resulting change of the current−voltage characteristics, on account of the passage of a bioanalyte, is fundamental in nanochannel sensing of the bioanalyte;[4,45−47] our study describes the fundamental nature of this base current (or base state current−voltage characteristics), including the highly interesting inversion of the base current, which, in turn, will help fabricate a much more efficient PE-grafted nanochannel sensor for biosensing applications.

SCALING LAWS FOR A POLYELECTROLYTE-GRAFTED NANOCHANNEL

We consider a nanochannel (height $2h$) grafted with a PE layer (thickness d and grafting density σ) on each of its walls. The PE layer can be either negative (see Figure 1a) or positively charged (see Figure 1b). We shall derive the scaling laws for this nanochannel, but prior to that, we repeat some of the well-known concepts on scaling of polymer brushes and the

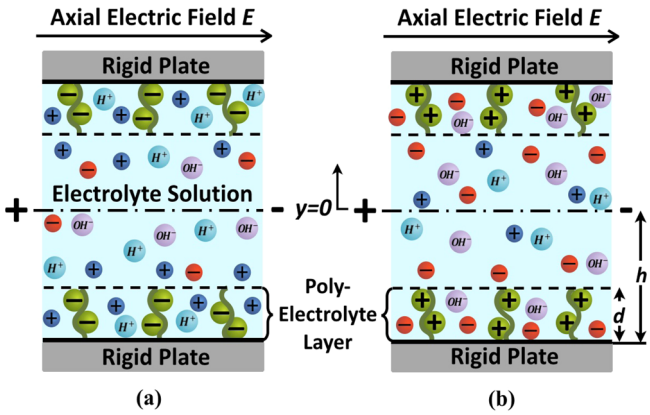

Figure 1. Schematic of the nanochannel grafted with (a) negatively charged PE layer and (b) positively charged PE layer. The schematic also shows the direction of the applied electric field that triggers the nanochannel ionic current.

selection of the equilibrium thickness d_{PB} of the polymer brushes.[48−52] All grafted polymer systems do not form brushes; rather brushes are formed only when the separation between the two adjacent grafted polymer layers (quantified as $\sigma^{-1/2}$) is smaller than a critical separation distance. This critical distance, quantified as $\sigma^{*-1/2}$ (i.e., the corresponding grafting density is σ^*), should be such that once the separation distance becomes smaller than this value the adjacent grafted chains will start interacting with each other. As has been hypothesized by several other researchers,[51,52] this critical distance, therefore, should be equal to the radius of gyration of the polymer chain $R \approx aN^{\nu}$ (where a is the polymer Kuhn length, N is the number of monomers in the polymer chain, and $\nu = 3/5$ for the case when the chain is in a "good" solvent). Therefore

$$\sigma^{*-1/2} \approx aN^{3/5} \Rightarrow \sigma^* \approx a^{-2}N^{-6/5} \tag{1}$$

Hence to ensure that the polymer grafting leads to the formation of brushes, one must have $\sigma > \sigma^*$. Please note that throughout this paper we shall consider the Kuhn length as a constant, specific to the polymer or PE. In other words, we do not account for the contribution of the electrostatic effects in altering the persistence length for a PE.[53−57]

For a grafted polymer chain in a brush-like configuration (with a brush height equal to d_{PB}), the free energy can be expressed as

$$\delta F_{PB} = \Delta F_{PB,ent} + \Delta F_{PB,VE} \approx k_B T\left[\frac{d_{PB}^2}{Na^2} + wN\left(\frac{N\sigma}{d_{PB}}\right)\right] \tag{2}$$

In eq 2, k_BT is thermal energy and w is the excluded volume parameter. Furthermore, the individual free-energy contributions are the entropic or chain stretching contribution ($\Delta F_{PB,ent}$) and the excluded volume contribution ($\Delta F_{PB,VE}$). Finally, the equilibrium height $d_{eq,PB}$ can be obtained by minimizing eq 2 with respect to d_{PB}

$$d_{eq,PB}N(w\sigma a^2)^{1/3} \tag{3}$$

Equation 3 yields the well-known scaling law for the polymer brush, where the brush thickness scales linearly with the polymer size N.[48−52]

With this preliminary background on the scaling concepts of polymer brushes, we now focus our attention to the present

DOI: 10.1021/acs.jpcb.5b07167
J. Phys. Chem. B XXXX, XXX, XXX−XXX

issue of scaling for the case of nanochannels grafted with PE brushes. Here there are two issues that are different from the simple scaling ideas of polymer brushes introduced above. They are (a) consideration of charges on the polymer (making it a PE), which, in turn, triggers the formation of an EDL of electrolyte ions around the PE molecule, and (b) selection of appropriate N and σ such that the resulting brush height remains smaller than the nanochannel half height.

For a single PE brush, the net free-energy change is composed of the free-energy changes associated with the grafted PE molecules as well as the induced EDL. Consequently

$$\Delta F = \Delta F_{\mathrm{PEB}} + \Delta F_{\mathrm{EDL}} = \Delta F_{\mathrm{PEB,ent}} + \Delta F_{\mathrm{PEB,VE}} + \Delta F_{\mathrm{PEB,elec}} + \Delta F_{\mathrm{EDL}} \tag{4}$$

In eq 4, $\Delta F_{\mathrm{PEB,ent}}$, $\Delta F_{\mathrm{PEB,VE}}$, and $\Delta F_{\mathrm{PEB,elec}}$ are the free-energy changes associated with the entropic, excluded volume, and electrostatic effects of the PE molecule, whereas ΔF_{EDL} is the free-energy change associated with the induced EDL. Before proceeding to use eq 4 to obtain the equilibrium height of the PE brushes, we shall first like to obtain the scaling for $\Delta F_{\mathrm{PEB,elec}}$. Assuming that an electrostatic potential of average magnitude ψ_0 has been triggered around the vicinity of a single grafted PE molecule, we may write $\Delta F_{\mathrm{PEB,elec}}$ for that PE molecule as

$$\Delta F_{\mathrm{PEB,elec}} \approx eN_{\mathrm{ch}}\psi_0 \tag{5}$$

where e is the electronic charge and N_{ch} is the total number of chargeable sites within the PE molecule. Typically, the connection between N_{ch} and N is expressed as

$$N_{\mathrm{ch}} = f_{\mathrm{ch}}N \tag{6}$$

where f_{ch} ($0 < f_{\mathrm{ch}} < 1$) represents the fraction of monomers that are charged.[52,58] Considering ψ_0 to be some multiple (not too small or not too large) of $k_{\mathrm{B}}T/e$ (this is also evident from the actual variation of the electrostatic potential, shown later) and using eq 6 under the condition of $f_{\mathrm{ch}} \approx 1$, we may rewrite eq 7 as

$$\Delta F_{\mathrm{PEB,elec}} \approx k_{\mathrm{B}}\mathrm{TN} \tag{7}$$

We next try to find out—through scaling arguments—the conditions that will allow us to use eq 3 even for the height d of the PE brush. In other words, these conditions will ensure that the electrostatic contribution of the grafted PE molecule will not contribute to the selection of the PE brush height, which, just like the case of uncharged polymer brushes, continues to be selected by the balance of the elastic and the excluded volume effects. To identify this condition, we take the ratio of $\Delta F_{\mathrm{PEB,elec}}$ and $\Delta F_{\mathrm{PEB,ent}}$, yielding

$$\frac{\Delta F_{\mathrm{PEB,elec}}}{\Delta F_{\mathrm{PEB,ent}}} \approx \frac{N^2a^2}{d^2} \tag{8}$$

Using eq 3 to replace d in eq 8 (the reasons are expressed above), we may write

$$\frac{\Delta F_{\mathrm{PEB,elec}}}{\Delta F_{\mathrm{PEB,ent}}} \approx \left(\frac{a}{\sigma w}\right)^{2/3} \tag{9}$$

Considering the Kuhn segment to be cylindrical (of thickness t), so that $w \approx a^2$t, we may rewrite eq 9 as

$$\frac{\Delta F_{\mathrm{PEB,elec}}}{\Delta F_{\mathrm{PEB,ent}}} \approx \left(\frac{1}{\sigma at}\right)^{2/3} \tag{10}$$

Equation 10 provides the critical value of the grafting density, referred to as σ_c, which dictates the relative influence of the electrostatic and the entropic effects of the grafted PE molecule, which, in turn, dictates whether the electrostatic effects of the PE molecule influence the selection of the PE brush height. From eq 10, we can express σ_c as [definition of σ_c is that $\left(\frac{\Delta F_{\mathrm{PEB,elec}}}{\Delta F_{\mathrm{PEB,ent}}}\right)_{\sigma=\sigma_c} \approx 1$]

$$\sigma_c \approx \frac{1}{at} \tag{11}$$

Therefore, the PE electrostatic effects become comparable to the entropic (and excluded volume effects) only when $\sigma \approx \sigma_c$. This is the case for which the PE electrostatic effects will influence the selection of the PE brush height, assumed to be selected by the balance of the entropic and the excluded volume effects of the PE. On the contrary, for $\sigma \ll \sigma_c$, $\Delta F_{\mathrm{PEB,elec}} \gg \Delta F_{\mathrm{PEB,ent}}$, whereas for $\sigma \gg \sigma_c$, $\Delta F_{\mathrm{PEB,elec}} \ll \Delta F_{\mathrm{PEB,ent}}$. For both of these cases (i.e., $\sigma \ll \sigma_c$ and $\sigma \gg \sigma_c$), we can consider a decoupled regime; that is, the electrostatic effects do not influence the selection of the PE brush thickness. Please note that with an increase in the grafting density (σ), there is no change in $\Delta F_{\mathrm{PEB,elec}}$. The change occurs, on the contrary, to $\Delta F_{\mathrm{PEB,ent}}$ and $\Delta F_{\mathrm{PEB,VE}}$. Enhanced σ enhances $\Delta F_{\mathrm{PEB,VE}}$ (see eq 2); physically this can be justified by following the argument of Milner.[51] Increase in the grafting density (σ) enforces an enhanced stretching of the grafted PE chain, which, in turn, allows it a more enhanced contact with the solvent avoiding contact with itself; for a good solvent (as is the case here), this tendency is preferred, leading to an enhancement of $\Delta F_{\mathrm{PEB,VE}}$. To balance this enhanced excluded volume energy, the elastic (or entropic) energy will also have to increase; an enhanced brush height indicates a larger stretching and hence a larger value of the elastic energy. (See eq 2.) Therefore, enhanced σ enhances $\Delta F_{\mathrm{PEB,ent}}$, justifying the condition that for $\sigma \gg \sigma_c$, $\Delta F_{\mathrm{PEB,elec}} \ll \Delta F_{\mathrm{PEB,ent}}$. Of course, this enhancement of both $\Delta F_{\mathrm{PEB,VE}}$ and $\Delta F_{\mathrm{PEB,ent}}$ with σ will imply that the equilibrium value of the free energy (or the minimized value of the free energy) also increases with σ; this is clearly evident by noting that this equilibrium energy is $\Delta F_{\mathrm{PB,eq}} \approx (\Delta F_{\mathrm{PB,ent}})_{d=d_{\mathrm{eq,PB}}} \approx (\Delta F_{\mathrm{PB,VE}})_{d=d_{\mathrm{eq,PB}}} \approx k_{\mathrm{B}}TNw^{2/3}\sigma^{2/3}a^{-2/3} \approx k_{\mathrm{B}}TNa^{2/3}t^{2/3}\sigma^{2/3}$ (obtained by using eq 3 in eq 2 and $w \approx a^2t$).

Because $\sigma \approx l^{-2}$ (where l is the distance of separation between the adjacent grafted PE chains), eq 11 also allows us to identify the decoupled regime in terms of the critical distance of separation. Please note that in the entire derivation of identifying σ_c, we have not accounted for ΔF_{EDL} The reason is straightforward. It is the PE charge (and the PE electrostatic effects) that triggers this EDL formation and the subsequent free-energy change. Therefore, ΔF_{EDL} should scale as $\Delta F_{\mathrm{PEB,elec}}$. Hence it suffices to represent the scaling of the entire electrostatic effects (i.e., the combination of the PE electrostatic effect and the EDL effects) by considering only $\Delta F_{\mathrm{PEB,elec}}$.

For the case where there is no constraint on the height of the PE brush (e.g., PE brush grafted to an interface in an unbounded electrolyte solution), eqs 1 and 11 suffice to pinpoint the conditions on the grafting density that must be obeyed to simultaneously ensure the formation of a brush-like structure as well as the attainment of decoupled (or coupled) regimes; however, in the present case, we are studying the PE-grafted nanochannels. Therefore, there needs to be an additional constraint that the PE brush height (d) should not exceed the channel half height (h). The condition $d > h$ will

DOI: 10.1021/acs.jpcb.5b07167
J. Phys. Chem. B XXXX, XXX, XXX−XXX

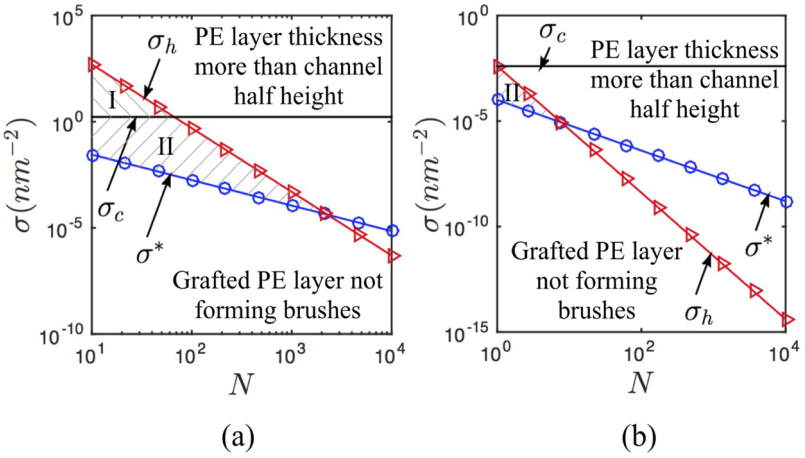

Figure 2. Variation of σ^*, σ_h, and σ_c with N for (a) grafted PAA chains and (b) grafted λ-DNA chains. The hashed zones in both the plots represent the $\sigma-N$ phase space that simultaneously ensure $d < h$ and that the grafted PEs form brush-like configurations. Also, these hashed zones are divided into zone I (where $\sigma > \sigma_c$ and hence $\Delta F_{PEB,elec} < \Delta F_{PEB,ent}$) and zone II (where $\sigma < \sigma_c$, and hence $\Delta F_{PEB,elec} > \Delta F_{PEB,ent}$). In these simulations, we use a = 1.5 nm[59] and t = 0.4 nm[60] for PAA chains, whereas a = 100 nm and t = 2.5 nm for DNA chains. Also, σ_h is computed for the both the cases considering h = 100 nm.

lead to a number of new physical phenomena (such as interdigitation and compression of PE brushes from the two nanochannel walls and so on.[29,30]), which is beyond the scope of the present analysis. To ensure $d < h$, we must have (using $w \approx a^2 t$ and assuming that we are in decoupled regime; that is, the PE brush thickness d is dictated by eq 3)

$$N(\sigma a^4 t)^{1/3} < h \tag{12}$$

The corresponding critical σ (denoted as σ_h), should therefore be

$$\sigma_h \approx \frac{h^3}{N^3 a^4 t} \tag{13}$$

By definition, σ_h denotes the critical grafting density that decides whether the PE layer thickness exceeds the nanochannel half height. In the case $\sigma < \sigma_h$, the PE layer thickness is smaller than the nanochannel height; on the other hand, if $\sigma > \sigma_h$, the PE thickness is greater than the nanochannel half height. Hence, within the scope of the present study, we must always have $\sigma < \sigma_h$.

From the above analysis, we may infer that three conditions (eqs 1, 11, and 13) simultaneously dictate the eventual choice of σ and the physical regime (brush or not, decoupled or not, entangled or not) in which the operation of the PE-grafted nanochannels can be categorized.

To illustrate the applicability of these scaling predictions and the manner in which these predictions allow us to chose our system parameters, we consider two actual examples of PE-grafted nanochannels. In the first example, we consider the PE to be the PAA, whereas in the second example, we consider the PE to be a DNA molecule. The results are illustrated in Figure 2a,b. These figures serve as the phase space for selecting the appropriate combination of N and σ values that will simultaneously ensure that the grafted PE molecules attain brush-like configuration and at the same time have a thickness d that is smaller than the nanochannel half height, h. For example, brush-like configuration is not satisfied for any $\sigma-N$ combination below the line representing the variation of σ^* with N; similarly, the brush formed will have a height larger than h for any $\sigma-N$ combination above the line representing the variation of σ_h with N. Therefore, both of these conditions (i.e., grafted PEs attain brush-like configuration and $d < h$) are simultaneously satisfied only by that $\sigma-N$ combination that lies within the hashed zones in both Figure 2a,b. Of course, the hashed zone that is below the line representing the variation of σ_c with N (please note that σ_c does not depend on N and hence is a line parallel to N axis) is the zone where $\Delta F_{PEB,elec} > \Delta F_{PEB,ent}$ (zone II), whereas the zone above this σ_c is zone I, where $\Delta F_{PEB,elec} < \Delta F_{PEB,ent}$. We find that while both of these zones exist for PAA, for DNA only zone II exists. To ensure that one works in the decoupled regime, one needs to choose a $\sigma-N$ combination that lies deep into any of these two zones well away from the σ_c line. Comparing Figure 2a,b, we can infer that the two conditions (formation of brush and $d < h$) are met only for a narrow window of values of σ and N (in fact for very small N) for the DNA chains, whereas for the PAA chains it is satisfied over a much broader ranges of these parameters. Such phase space created on the basis of our scaling calculations is useful for designing of PE-grafted nanochannels and for pinpointing the dominant effects that govern the functioning of these nanochannels.

pH-DEPENDENT ELECTROSTATICS AND IONIC CURRENT IN A PE-GRAFTED NANOCHANNEL

We are interested to obtain the electrostatics and the ionic current in a PE-grafted nanochannel for the case where the PE layer thickness d is independent of the electrostatic effects. In other words, we consider a $\sigma-N$ combination of the grafted PE molecules that is in the hashed zone. (See Figure 2a,b.) A logical choice can be PAA molecules with N = 100 and $\sigma = 10^{-2}$ nm^{-2}. This ensures that the parameters belong to the hashed zone II and substantially away from the line quantifying the σ_c variation with N (see Figure 2a); for such a choice, $\sigma \ll \sigma_c$ and hence $\Delta F_{PEB,elec} \gg \Delta F_{PEB,ent}$. Please note that the analysis that follows is always valid for a nanochannel grafted PE brush system with $\sigma \ll \sigma_c$ (i.e., $\Delta F_{PEB,elec} \gg \Delta F_{PEB,ent}$). Of course, almost identical analysis of the PE layer electrostatics is valid for the other zone (zone I, where $\sigma \gg \sigma_c$ and hence $\Delta F_{PEB,elec} \ll \Delta F_{PEB,ent}$); the only difference is that for this case the contribution of $\Delta F_{PEB,elec}$ in the overall ΔF_{PEB} is negligible.

For the case where we are in zone II, we may write

DOI: 10.1021/acs.jpcb.5b07167
J. Phys. Chem. B XXXX, XXX, XXX−XXX

$$\Delta F \approx \Delta F_{\mathrm{PEB,elec}} + \Delta F_{\mathrm{EDL}} = \int f(\psi, \psi', n_{\pm}, n_{\mathrm{H}^+}, n_{\mathrm{OH}^-}) d^3\mathbf{r} \tag{14}$$

Here f is the density of the free energy change, expressed as

$$f = k_{\mathrm{B}}T \sum_i \left[n_i \left(\ln\left(\frac{n_i}{n_{i,\infty}}\right) - 1 \right) \right] - \frac{\epsilon_0 \epsilon_r}{2} |\nabla\psi|^2 + e\psi\left[\sum_i z_i n_i - \varphi n_{\mathrm{A}^-}\right]$$
$$(-h \le y \le -h + d) \text{ (negative PE layer)},$$
$$f = k_{\mathrm{B}}T \sum_i \left[n_i \left(\ln\left(\frac{n_i}{n_{i,\infty}}\right) - 1 \right) \right] - \frac{\epsilon_0 \epsilon_r}{2} |\nabla\psi|^2 + e\psi\left[\sum_i z_i n_i + \varphi n_{\mathrm{BH}^+}\right]$$
$$(-h \le y \le -h + d) \text{ (positive PE layer)},$$
$$f = k_{\mathrm{B}}T \sum_i \left[n_i \left(\ln\left(\frac{n_i}{n_{i,\infty}}\right) - 1 \right) \right] - \frac{\epsilon_0 \epsilon_r}{2} |\nabla\psi|^2 + e\psi\left[\sum_i z_i n_i\right]$$
$$(-h + d \le y \le 0) \tag{15}$$

In eq 15, in the right-hand side the first term represents the entropic contribution of the ions, the second term represents the self-electrostatic energy of the EDL electric field, and the final term represents the electrostatic energy of the electrolyte, hydrogen, hydroxyl, and the PE ions. (The contribution due to the PE ions is absent for $-h + d \le y \le 0$.) Further ψ is the electrostatic potential, ϵ_0 is the permittivity of free space, ϵ_r is the relative permittivity of the medium, e is the electronic charge, and n_i and $n_{i,\infty}$ are the number density and the bulk number density of i ($i = \pm$, H^+, OH^-). Here the electrolyte salt is assumed to be monovalent and symmetric. z_i is the valence of the ionic species i ($i = \pm$, H^+, OH^-). Also in eq 15, n_{A^-} and n_{BH^+} are the number densities of the positive and negative PE ions. Furthermore, $\varphi(y)$ is the dimensionless monomer distribution.[12] Following Chen and Das,[12,13] we can express $\varphi(y)$ to be a nonunique cubic function in y; this ensures avoiding unphysical discontinuities associated with considering a constant φ for a PE layer with pH(pOH)-dependent charge density.[12] The number densities of the PE ions depend on local H^+ (or OH^-) ion concentration values for negative (positive) PE layer and can be expressed as

$$n_{\mathrm{A}^-} = \frac{K_{\mathrm{a}}' \gamma_{\mathrm{a}}}{K_{\mathrm{a}}' + n_{\mathrm{H}^+}}, \quad n_{\mathrm{BH}^+} = \frac{K_{\mathrm{b}}' \gamma_{\mathrm{b}}}{K_{\mathrm{b}}' + n_{\mathrm{OH}^+}} \tag{16}$$

Here the anionic charge of the negatively charged PE layer is attributed to the ionization of the acid HA ($\mathrm{HA} \leftrightarrow \mathrm{H}^+ + \mathrm{A}^-$; ionization constant K_{a}), whereas the cationic charge of the positively charged PE layer is attributed to the ionization of base B ($\mathrm{B} + \mathrm{H_2O} \leftrightarrow \mathrm{BH}^+ + \mathrm{OH}^-$; ionization constant K_{b}). Also, in eq 16, γ_{a} and γ_{b} are the maximum site densities of anionic (for the negatively charged PE layer) and the cationic (for the positively charged PE layer) groups, and $K_{\mathrm{a}}' = 10^3 N_{\mathrm{A}} K_{\mathrm{a}}$, $K_{\mathrm{b}}' = 10^3 N_{\mathrm{A}} K_{\mathrm{b}}$ (N_{A} is Avogadro's number). Please note that eq 15 is based on the assumption that the EDL can be described by the mean-field electrostatics. Therefore, issues such as ion−ion correlations have not been considered. In fact, effects such as consideration of finite ion sizes and finite solvent polarizability (these effects can be modeled within the mean-field framework) have also been neglected.

To obtain the equilibrium distribution of the electrostatic potential and the ionic distribution for the present case (described by eqs 15 and 16), we minimize eq 15 with respect to ψ, $n_{\pm}$, n_{H^+}, and n_{OH^-}. The minimization yields coupled ordinary differential equations for ψ and n_{H^+} (or n_{OH^-}) for negative (or positive) PE layer, which are solved numerically to obtain the equilibrium profiles of ψ, n_{H^+} (or n_{OH^-}), and φn_{A^-} (or $\varphi n_{\mathrm{BH}^+}$). Please note that in our previous paper[12] this minimization procedure has been discussed in great detail for negatively charged PE layers; here we briefly summarize these steps and also provide the minimization steps for the positively charged PE layer.

Negatively Charged PE Layer. The equilibrium electrostatic potential and the concentration distribution of different ions can be obtained by minimizing ΔF (see eqs 14 and 15 for expression of ΔF) with respect to ψ, $n_{\pm}$, n_{H^+}, and n_{OH^-}.

By minimizing ΔF with respect to ψ yields

$$\frac{\delta(\Delta F)}{\delta\psi} = 0 \Rightarrow \frac{\partial f}{\partial \psi} - \frac{\mathrm{d}}{\mathrm{d}y}\left(\frac{\partial f}{\partial \psi'}\right) = 0 \Rightarrow \frac{\mathrm{d}^2\psi}{\mathrm{d}y^2} = \frac{e(n_- - n_+ + n_{\mathrm{OH}^-} - n_{\mathrm{H}^+} + \varphi n_{\mathrm{A}^-})}{\epsilon_0 \epsilon_r} \quad [\text{for } -h \le y \le -h + d]$$
$$\frac{\delta(\Delta F)}{\delta\psi} = 0 \Rightarrow \frac{\partial f}{\partial \psi} - \frac{\mathrm{d}}{\mathrm{d}y}\left(\frac{\partial f}{\partial \psi'}\right) = 0 \Rightarrow \frac{\mathrm{d}^2\psi}{\mathrm{d}y^2} = \frac{e(n_- - n_+ + n_{\mathrm{OH}^-} - n_{\mathrm{H}^+})}{\epsilon_0 \epsilon_r} \quad [\text{for } -h + d \le y \le 0] \tag{17}$$

Minimizing ΔF with respect to $n_{\pm}$, n_{H^+}, and n_{OH^-} yields

$$\frac{\delta(\Delta F)}{\delta n_{\pm}} = 0 \Rightarrow n_{\pm} = (n_{\pm,\infty}) \exp\left(\mp \frac{e\psi}{K_{\mathrm{B}}T}\right) [\text{for } y \ge -h] \tag{18}$$

$$\frac{\delta(\Delta F)}{\delta n_{\mathrm{OH}^-}} = 0 \Rightarrow n_{\mathrm{OH}^-} = (n_{\mathrm{OH}^-,\infty}) \exp\left(\frac{e\psi}{K_{\mathrm{B}}T}\right) [\text{for } y \ge -h] \tag{19}$$

and

$$\frac{\delta(\Delta F)}{\delta n_{\mathrm{H}^+}} = 0 \Rightarrow n_{\mathrm{H}^+} = (n_{\mathrm{H}^+,\infty}) \exp\left[-\frac{e\psi}{K_{\mathrm{B}}T}\left(1 + \varphi \frac{K_{\mathrm{a}}'\gamma_{\mathrm{a}}}{(K_{\mathrm{a}}' + n_{\mathrm{H}^+})^2}\right)\right] \quad [\text{for } -h \le y \le -h + d]$$
$$\frac{\delta(\Delta F)}{\delta n_{\mathrm{H}^+}} = 0 \Rightarrow n_{\mathrm{H}^+} = (n_{\mathrm{H}^+,\infty}) \exp\left(-\frac{e\psi}{K_{\mathrm{B}}T}\right) [\text{for } -h + d \le y \le 0] \tag{20}$$

Here $n_{\pm,\infty}$ are the bulk number densities of the electrolyte ions (in units of $1/m^3$), $n_{\mathrm{H}^+,\infty} = 10^{3-\mathrm{pH}_\infty} N_{\mathrm{A}}$ (pH_∞ is the bulk pH) is the bulk number density of hydrogen ions, $n_{\mathrm{OH}^-,\infty} = 10^{3-\mathrm{pOH}_\infty} N_{\mathrm{A}}$ (pOH_∞ is the bulk pOH) is the bulk number density of the hydroxide ions and $\mathrm{pH}_\infty + \mathrm{pOH}_\infty = 14$. Here $n_{+,\infty} = n_\infty$ and $n_{-,\infty} = n_\infty + n_{\mathrm{H}^+,\infty}$. Here n_∞ is the bulk number density of the electrolyte ions contributed by the added electrolyte salt; n_∞ is related to the bulk concentration c_∞ (in M) as $n_\infty = 10^3 N_{\mathrm{A}} c_\infty$. More importantly, here we assume that the added acid furnishes the same anion as the electrolyte salt. The bulk number densities are the number densities of the ions in the microchannel reservoirs (where $\psi = 0$) connecting the nanochannel.[61−63] Solution of ψ can be obtained by first using eqs 18−20 to replace the ion number densities appearing in eq 17 and then solving the resultant differential equation in ψ in the presence of the boundary conditions expressed in eq 21

DOI: 10.1021/acs.jpcb.5b07167
J. Phys. Chem. B XXXX, XXX, XXX−XXX

$$\left(\frac{d\psi}{dy}\right)_{y=0} = 0,\ (\psi)_{y=(-h+d)^+} = (\psi)_{y=(-h+d)^-},$$
$$\left(\frac{d\psi}{dy}\right)_{y=(-h+d)^+} = \left(\frac{d\psi}{dy}\right)_{y=(-h+d)^-},\ \left(\frac{d\psi}{dy}\right)_{y=-h} = 0 \quad (21)$$

The critical thing to note here is that this differential equation in ψ (see eq 22 for the corresponding dimensionless form) will also contain the unresolved expression for n_{H^+}; this stems from the fact that while the expressions for the number densities of all other ions (i.e., $n_{\pm}$, n_{OH^-}) are explicit in ψ (see eqs 18 and 19), n_{H^+} is implicit in ψ. (See eq 20 and note the fact that n_{H^+} also appears in the right-hand side of the first equation of eq 20.) Therefore, we shall have a set of equations for ψ and n_{H^+} that needs to be solved simultaneously. These equations, in dimensionless forms, can be expressed as

$$\frac{d^2\bar{\psi}}{d\bar{y}^2} = \frac{1}{2\bar{\lambda}^2}\left[(1+\bar{n}_{H^+,\infty})\exp(\bar{\psi}) - \exp(-\bar{\psi}) + \bar{n}_{OH^-,\infty}\exp(\bar{\psi}) - \bar{n}_{H^+} + \frac{\overline{K_a'}\bar{\gamma}_a\varphi(\bar{y})}{\overline{K_a'} + \bar{n}_{H^+}}\right] [\text{for } -1 \le \bar{y} \le -1+\bar{d}]$$
$$\frac{d^2\bar{\psi}}{d\bar{y}^2} = \frac{1}{2\bar{\lambda}^2}[(1+\bar{n}_{H^+,\infty})\exp(\bar{\psi}) - \exp(-\bar{\psi}) + \bar{n}_{OH^-,\infty}\exp(\bar{\psi}) - \bar{n}_{H^+,\infty}\exp(-\bar{\psi})] \ [\text{for } -1+\bar{d} \le \bar{y} \le 0] \quad (22)$$

$$\bar{\psi} = -\frac{\ln\left(\frac{\bar{n}_{H^+}}{\bar{n}_{H^+,\infty}}\right)}{1 + \frac{\overline{K_a'}\bar{\gamma}_a\varphi(\bar{y})}{(\overline{K_a'} + \bar{n}_{H^+})^2}} \ [\text{for } -1 \le \bar{y} \le -1+\bar{d}]$$
$$\bar{\psi} = -\ln\left(\frac{\bar{n}_{H^+}}{\bar{n}_{H^+,\infty}}\right) [\text{for } -1+\bar{d} \le \bar{y} \le 0] \quad (23)$$

The corresponding dimensionless boundary conditions become

$$\left(\frac{d\bar{\psi}}{d\bar{y}}\right)_{\bar{y}=0} = 0,\ (\bar{\psi})_{\bar{y}=(-1+\bar{d})^+} = (\bar{\psi})_{\bar{y}=(-1+\bar{d})^-},$$
$$\left(\frac{d\bar{\psi}}{d\bar{y}}\right)_{\bar{y}=(-1+\bar{d})^+} = \left(\frac{d\bar{\psi}}{d\bar{y}}\right)_{\bar{y}=(-1+\bar{d})^-},\ \left(\frac{d\bar{\psi}}{d\bar{y}}\right)_{\bar{y}=-1} = 0 \quad (24)$$

In the above equations, $\bar{y} = y/h$, $\bar{\lambda} = \lambda/h$ ($\lambda = \sqrt{\frac{\epsilon_0\epsilon_r K_B T}{2n_\infty e^2}}$ is the EDL thickness), $\bar{d} = d/h$, $\bar{\psi} = e\psi/(k_B T)$, $\bar{n}_{H^+} = n_{H^+}/n_\infty$, $\bar{n}_{OH^-} = n_{OH^-}/n_\infty$, $\bar{n}_{H^+,\infty} = n_{H^+,\infty}/n_\infty$, $\bar{n}_{OH^-,\infty} = n_{OH^-,\infty}/n_\infty$, $\overline{K_a'} = K_a'/n_\infty$, and $\bar{\gamma}_a = \gamma_a/n_\infty$. Also as established in our previous studies,[12,13] φ has a spatially cubic profile, expressed as

$$\varphi(\bar{y}) = \beta(\bar{y} + 1 - \bar{d})^2\left(\bar{y} + 1 + \frac{\bar{d}}{2}\right) \quad (25)$$

where $\beta = 4/\bar{d}^3$. Under these conditions, the explicit equilibrium electrostatic potential and hydrogen ion concentration distribution can be obtained by numerically solving the coupled eqs 22 and 23 in the presence of the boundary condition expressed in eq 24.

Positively Charged PE Layer. For positively charged PE layer, we have $n_{-,\infty} = n_\infty$ and $n_{+,\infty} = n_\infty + n_{OH^-,\infty}$. This is under the assumption that bulk number density of the electrolyte ions contributed by the added electrolyte salt is n_∞, and the base added produces the same cations as the added salt. For this case, too, the same minimization procedure (i.e., minimizing ΔF with respect to ψ, $n_{\pm}$, n_{H^+}, and n_{OH^-}) is employed. Here n_{OH^-} depends on ψ implicitly (see eq 28 and note the fact that n_{OH^-} also appears in the right-hand side of the first equation of eq 28), while the dependence of $n_{\pm}$ and n_{H^+} on ψ is explicit. The resulting set of equations

$$\frac{\delta(\Delta F)}{\delta\psi}0 \Rightarrow \frac{\partial f}{\partial\psi} - \frac{d}{dy}\left(\frac{\partial f}{\partial\psi'}\right) = 0 \Rightarrow \frac{d^2\psi}{dy^2} = \frac{e(n_- - n_+ + n_{OH^-} - n_{H^+} - \varphi n_{BH^+})}{\epsilon_0\epsilon_r} \ [\text{for } -h \le y \le -h+d]$$
$$\frac{\delta(\Delta F)}{\delta\psi} = 0 \Rightarrow \frac{\partial f}{\partial\psi} - \frac{d}{dy}\left(\frac{\partial f}{\partial\psi'}\right) = 0 \Rightarrow \frac{d^2\psi}{dy^2} = \frac{e(n_- - n_+ + n_{OH^-} - n_{H^+})}{\epsilon_0\epsilon_r} \ [\text{for } -h+d \le y \le 0] \quad (26)$$

$$\frac{\delta(\Delta F)}{\delta n_{H^+}} = 0 \Rightarrow n_{H^+} = (n_{H^+,\infty})\exp\left(-\frac{e\psi}{k_B T}\right) [y \ge -h] \quad (27)$$

$$\frac{\delta(\Delta F)}{\delta n_{OH^-}} = 0 \Rightarrow n_{OH^-} = (n_{OH^-,\infty})\exp\left[\frac{e\psi}{k_B T}\left(1 + \varphi\frac{K_b'\gamma_b}{(K_b' + n_{OH^-})^2}\right)\right] \ [\text{for } -h \le y \le -h+d]$$
$$\frac{\delta(\Delta F)}{\delta n_{OH}} = 0 \Rightarrow n_{OH} = (n_{OH,\infty})\exp\left(\frac{e\psi}{k_B T}\right) [\text{for } -h+d \le y \le 0] \quad (28)$$

Finally, the electrolyte ion concentrations are governed by eq 18. Consequently, the resulting set of coupled governing equations will be in ψ and n_{OH^-}. They are expressed in dimensionless form as

$$\frac{d^2\bar{\psi}}{d\bar{y}^2} = \frac{1}{2\bar{\lambda}^2}\left[\exp(\bar{\psi}) - (1+\bar{n}_{OH^-,\infty})\exp(-\bar{\psi}) - \bar{n}_{H^+,\infty}\exp(-\bar{\psi}) + \bar{n}_{OH^-} - \frac{\overline{K_b'}\bar{\gamma}_b\varphi(\bar{y})}{\overline{K_b'} + \bar{n}_{OH^-}}\right] [\text{for } -1 \le \bar{y} \le -1+\bar{d}]$$
$$\frac{d^2\bar{\psi}}{d\bar{y}^2} = \frac{1}{2\bar{\lambda}^2}[\exp(\bar{\psi}) - (1+\bar{n}_{OH^-,\infty})\exp(-\bar{\psi}) - \bar{n}_{H^+,\infty}\exp(-\bar{\psi}) + \bar{n}_{OH^-,\infty}\exp(\bar{\psi})] \ [\text{for } -1+\bar{d} \le \bar{y} \le 0] \quad (29)$$

$$\bar{\psi} = \frac{\ln\left(\frac{\bar{n}_{OH^-}}{\bar{n}_{OH^-,\infty}}\right)}{1 + \frac{\overline{K_b'}\bar{\gamma}_b\varphi(\bar{y})}{(\overline{K_b'} + \bar{n}_{OH^-})^2}} \ [\text{for } -1 \le \bar{y} \le -1+\bar{d}]$$
$$\bar{\psi} = \ln\left(\frac{\bar{n}_{OH^-}}{\bar{n}_{OH^-,\infty}}\right) [\text{for } -1+\bar{d} \le \bar{y} \le 0] \quad (30)$$

In the above equations, $\bar{\gamma}_b = \gamma_b/n_\infty$ and $\overline{K_b'} = K_b'/n_\infty$. Under these conditions and using eq 25 to express φ, the explicit equilibrium electrostatic potential and hydroxide ion concentration distribution can be obtained by numerically solving the coupled eqs 29 and 30 in the presence of the boundary condition expressed in eq 24.

DOI: 10.1021/acs.jpcb.5b07167
J. Phys. Chem. B XXXX, XXX, XXX−XXX

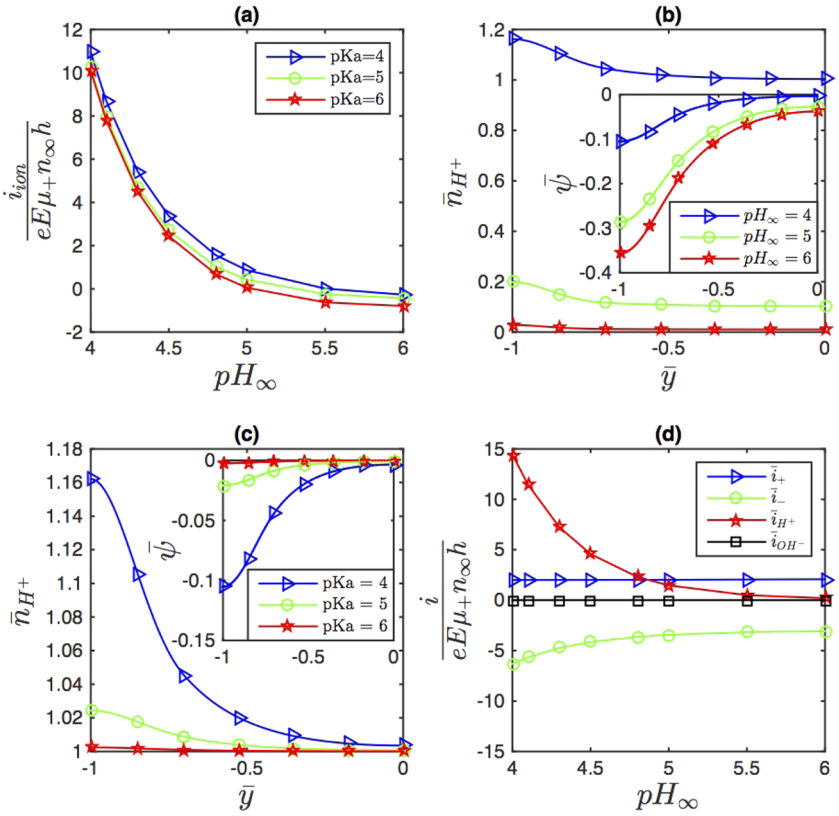

Figure 3. (a) Variation of the ionic current with pH_∞ for different values of pK_a for a negatively charged PE layer. Here we consider the electrolyte salt as NaCl and the acid as HCl. The relevant unsigned mobility values are $\mu_+ = \mu_{Na^+} = 5 \times 10^{-8}$ m^2/(V s), $\mu_- = \mu_{Cl^-} = 7.9 \times 10^{-8}$ m^2/(V s), $\mu_{H^+} = 36 \times 10^{-8}$ m^2/(V s), and $\mu_{OH^-} = 20 \times 10^{-8}$ m^2/(V s). (b) Variation of the dimensionless number density of H^+ ion ($\bar{n}_{H^+,\infty}$) and the dimensionless electrostatic potential ($\bar{\psi}$) (shown in the inset) with $\bar{y}$ for different values of pH_∞ for $pK_a = 4$. (c) Variation of the dimensionless number density of H^+ ion ($\bar{n}_{H^+,\infty}$) and the dimensionless electrostatic potential ($\bar{\psi}$) (shown in the inset) with $\bar{y}$ for different values of pK_a for $pH_\infty = 4$. (d) Variation of the dimensionless ionic currents with pH_∞ due to different ions [$\bar{i}_+ = \frac{i_+}{eE\mu_+ n_{\infty H}}$, $\bar{i}_- = \frac{i_-}{eE\mu_+ n_{\infty H}}$, $\bar{i}_{H^+} = \frac{i_{H^+}}{eE\mu_+ n_{\infty H}}$, $\bar{i}_{OH^-} = \frac{i_{OH^-}}{eE\mu_+ n_{\infty H}}$] for $pK_a = 6$. For all plots, we use $c_\infty = 10^{-4}$ M (i.e., $n_\infty = c_\infty \times N_A \times 10^3 = 6.023 \times 10^{22}$ L/m^3), $\gamma_a = 10^{-4}$ M, $\bar{d} = 0.3$, $h = 100$ nm, $k_B T = 4.14 \times 10^{-21}$ J, $e = 1.6 \times 10^{-19}$ C, $\epsilon_0 = 8.8 \times 10^{-12}$ F/m, and $\epsilon_r = 79.8$.

IONIC CURRENT IN A PE-GRAFTED NANOCHANNEL

Once the electrostatic potential has been computed, it can be employed to calculate the corresponding number density distribution n_i. Subsequently, we can obtain the ionic current (i_{ion}) as

$$i_{ion} = eE \int_{-h}^{h} \left[\sum_i \frac{z_i}{|z_i|} \mu_i n_i \right] dy \tag{31}$$

where μ_i is the unsigned electrophoretic mobility of species i ($i = \pm, H^+, OH^-$) and E is the electric field.

Figure 3a provides the variation of the ionic current with pH_∞ (or bulk pH). The ionic current, most remarkably, shows an inversion at large bulk pH. In other words, as pH_∞ increases, the ionic current first decreases from a positive value, becomes zero, and then attains a negative value. Along with the scaling laws for the nanochannel provided here, this is the other key finding of this paper. Here we consider a negatively charged PE layer; therefore this attainment of a negative value by the ionic current is the most amazing example of co-ion-dominated ionic current. We explain this highly nonintuitive ionic current variation by analyzing the corresponding variation of the electrostatic potential ($\bar{\psi}$) and the hydrogen ion number density ($\bar{n}_{H^+}$).

Because $|\bar{\psi}|$ is small (see Figure 3b,c), for the negative PE layer, we can express the ionic current as

$$\frac{i_{ion}}{eE} \approx \int_{-h}^{h} [n_\infty \mu_+ - (n_\infty + n_{H^+,\infty})\mu_- - n_{OH^-,\infty}\mu_{OH^-}]\, dy - \int_{-h}^{h} \bar{\psi}[n_\infty \mu_+ + (n_\infty + n_{H^+,\infty})\mu_- + n_{OH^-,\infty}\mu_{OH^-}]\, dy + \int_{-h}^{h} \mu_{H^+} n_{H^+}\, dy \tag{32}$$

Here the first integral represents the contribution of the bulk ionic mobilities, the second integral represents the contribution of ion mobilities due to the EDL effects, and the third integral represents both the EDL and the bulk mobility contributions of the hydrogen ions. In Figure 3d, we show the contribution of the ionic current due to individual ion types (+, −, H^+, and OH^-) to the overall ionic current as a function of pH_∞ for a given pK_a (= 6). For small pH_∞, H^+ ion concentration is large. (See Figure 3b.) This when coupled to the very large ionic mobility of the H^+ ions, a very large positive ionic current is triggered. (See Figure 3a,d.) Because the PE layer is negative, this is an example of counterion-dominated ionic current, which typically symbolizes a nanochannel ionic current.[13,64] Please note that here the magnitude of dimensionless electrostatic potential is very small (<1) and also $n_{+,\infty} < n_{-,\infty}$; consequently,

DOI: 10.1021/acs.jpcb.5b07167
J. Phys. Chem. B XXXX, XXX, XXX−XXX

the contribution of the salt counterions (here Na^+) in ensuring a counterion-dominated ionic current is less significant. (See Figure 3d.) Therefore, we encounter a very interesting situation where the counterion-dominated ionic current results not from the salt counterions, but from the H^+ ions of the acid. This is the first important facet of the variation of the ionic current. Increase in pH_∞ implies a decrease in the H^+ ion concentration, which, in turn, reduces the ionic current. Finally, at substantially large pH_∞ (i.e., large in comparison to the acidic pH), we encounter the most remarkable situation of negative ionic current. This signifies an inversion in the ionic current or, in other words, a co-ion-dominated ionic current. (Here Cl^- ion is the co-ion.) For such large pH_∞, because H^+ ion concentration is very small, the ionic current is dictated by the salt co-ions and counterions. Here the electrostatic potential is small, and it is the bulk value (and not the EDL-induced value) of the salt co-ion and counterion mobilities that dictate the overall ionic current. Because $n_{+,\infty} < n_{-,\infty}$ and $\mu_+ < \mu_-$, we get a negative value of the ionic current. This can further be established by simply noting the ionic current due to the individual ion types at large pH_∞ (see Figure 3d); at large pH_∞, the current due to the negative electrolyte ions dictates the overall current, thereby inverting the current and making it co-ion-dominated. In summary, in a PE layer-grafted nanochannel with pH-dependent charge density, we witness the highly nonintuitive pH-dependent ionic current inversion from a large positive value to a negative value signifying a switch from the more intuitive counterion-dominated EDL ionic current to the highly nonintuitive co-ion-dominated EDL ionic current. Figure 3a also demonstrates that unlike pH_∞ variation of pK_a has relatively little influence on the ionic current at a given pH_∞. At low pH_∞, H^+ ion concentration dictates the ionic current, and this H^+ ion concentration shows very little effect with the variation in pK_a. (See Figure 3c.) Similarly, at large pH_∞, $|\overline{\psi}|$ remains small irrespective of the pK_a value; consequently, the ionic mobility continues to be dictated by the bulk value of the co-ion mobility, resulting in a negative value of ionic current for all values of pK_a. Figure 4 provides a parametric variation of the nanochannel ionic current for the negatively charged PE layer. The relatively weak dependence of the ionic current variation with pK_a results in a relatively weak variation of the ionic current with the variation in the parameters associated with the PE layer (e.g., $\overline{\gamma}_a$ and $\overline{d}$). Of course, smaller $\overline{\gamma}_a$ and smaller $\overline{d}$ imply relatively weaker contribution of the PE charge; hence there is weaker accumulation of the hydrogen ions. Consequently, the ionic current decreases at a given pH_∞, resulting in a smaller positive value at a smaller pH_∞ and a larger negative value at a larger pH_∞. Most interesting variation is witnessed for larger salt concentration ($c_\infty = 10^{-3}$ M). For this case, the ionic current gets inverted at a much lower pH_∞; this results from the fact that the cause of ionic current inversion (i.e., the ionic current becoming dominated by the bulk mobility of the electrolyte co-ions) gets triggered at a much lower pH_∞ when the electrolyte concentration is large.

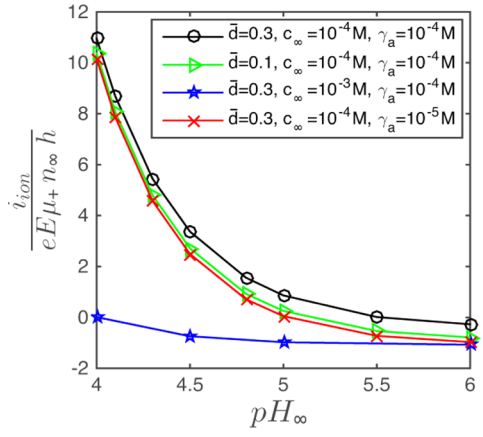

Figure 4. Variation of the ionic current with pH_∞ for a negatively charged PE layer for $pK_a = 4$ and for different values of $\overline{d}$, γ_a, and c_∞. Other parameters, including the unsigned mobility values of the different ions, are identical to those used in Figure 3.

The most important finding revealed by Figures 3a and 4 is the presence of the current inversion. As has been previously explained, the ionic current for large pH_∞ (i.e., when the effect of the ionic current due to the hydrogen and hydroxyl ions can be neglected) consists of two parts, namely, the bulk ionic current that results from the difference in mobilities (μ_i) of the electrolyte ions and the EDL-induced current dictated by the corresponding EDL-electrostatic-potential-induced differences in the ion number density distributions of the electrolyte ions. Current inversion signals a situation where the effect of the EDL-induced current is massively overwhelmed by the bulk current. This becomes possible only when the EDL electrostatic potential becomes weak enough to make the contribution of the EDL current negligible. Therefore, in terms of the net ionic current, such PE-grafted nanochannels can be considered to have negligible EDL influence for large bulk pH values.

Finally, in Figure 5, we show the variation of the ionic current for the positively charged PE layer. Here the ionic current shows no inversion; rather, it is always negative, indicating that the ionic current is always counterion-dominated. Here, too, however, at larger bulk pOH or pOH_∞, the current becomes dominated by the bulk ionic mobility of the electrolyte ions, but because the mobility of the counterions (here Cl^- ions) is more than that of co-ions (here Na^+ ions), we do not get any current inversion. Of course, from this analysis, we can easily predict that had we worked with a salt where the cationic mobility is more than the anionic mobility, we would have witnessed an ionic current inversion

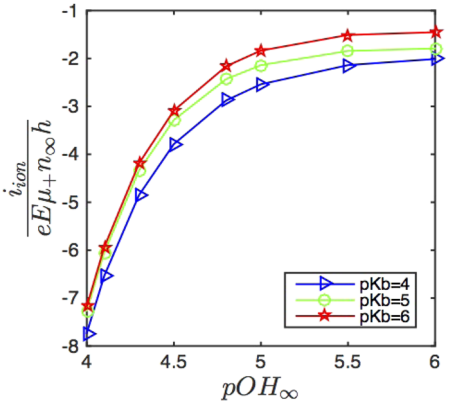

Figure 5. Variation of the ionic current with pOH_∞ for different values of pK_b for a positively charged PE layer. Here we consider the electrolyte salt as NaCl and the base as NaOH. The relevant unsigned mobility values for the different ions are provided in the caption of Figure 3. Also, $c_\infty = 10^{-4}$ M (i.e., $n_\infty = 6.023 \times 10^{22}$ L/m^3), $\gamma_b = 10^{-4}$ M, $\overline{d} = 0.3$, $h = 100$ nm, $k_BT = 4.14 \times 10^{-21}$ J, $e = 1.6 \times 10^{-19}$ C, $\epsilon_0 = 8.8 \times 10^{-12}$ F/m, and $\epsilon_r = 79.8$.

DOI: 10.1021/acs.jpcb.5b07167
J. Phys. Chem. B XXXX, XXX, XXX−XXX

(or a co-ion dominated current) for the positive PE layer and no current inversion for the negative PE layer.

DISCUSSION

Correlation of Our Model with Reported Experimental Studies. To the best of our knowledge there is no experimental study that has reported ionic current inversion in nanochannels (with or without PE grafting). Please note that our predicted ionic current inversion is not the same as the switching of the current direction caused by the charge inversion[31,32]-mediated switching of the sign of the electrostatic potential and the sign of the counterion charge (as witnessed by He et al.[65]). Charge inversion (CI) was discussed in the Introduction and is a phenomenon where the electrostatic potential in the vicinity of a charged wall has an electrostatic potential whose sign is opposite to that of the bare charge of the wall. The primary cause of such inversion is the presence of multivalent counterions[33−35] (and the resulting ionic correlation effects) or the presence of finite-sized co-ions and counterions.[36] Such multivalent-counterion-driven CI was witnessed in conical nanopores in the experiments of He et al.;[65] the presence of multivalent counterions like Ca^{2+} and Co^{3+} caused local CI, thereby changing the effective charge of the nanopore from negative to positive. This inversion of the effective nanopore charge inverted the sign of the electrostatic potential and therefore most intuitively switched the direction of the ionic current. Such switching of direction is not the current inversion that we report here. Current inversion occurs only when the current becomes co-ion-dominated; however, in experiments of He et al.[65] the current is always the standard case of counterion-dominated current, regardless of whether there is CI. For example, in the experiment of He et al.,[65] the surface charge of the conical nanopore, in absence of the multivalent cations, was negative. For this case, when a negative (positive) voltage was applied at the wider section of the conical nanopore and a ground was applied at the narrower section, the magnitude of the current increased (decreased). Please note that the convention used in this paper[65] considered the current to be positive if positive (negative) charges moved from right (left) to left (right), with the wider section being at the right and the narrower section being at the left. This clearly suggested that the current was counterion-driven because when the counterions were positive (as the surface charge of the nanopore was negative), a negative (positive) voltage at the wider section of the pore enhanced (lowered) the current. In the presence of large concentration of Co^{3+} ions (∼10 mM), the surface charge of the conical nanopore got inverted and became positive. For this case, a positive (negative) voltage at the wider section of the nanopore increased (decreased) the magnitude of the current. This, too, was an example of counterion-dominated ionic current; the surface charge of the nanopore was positive and the counterions were negatively charged and hence demonstrated a much enhanced magnitude of the current when a positive voltage was applied at the wider section of the conical nanopore. Such counterion-dominated current implied that the change in sign of the current, most intuitively, was caused by the CI-mediated change in the sign of the counterion charges and the corresponding change in the sign of the applied voltage (at the wider section of the nanopore). On the contrary, for our case for certain combination of parameters the current becomes co-ion-dominated and accordingly changes sign despite no change in the sign of the electrostatic potential or of the applied voltage. (See Figure 3a,b.) This is the unique scenario of current inversion that has not been reported in any other previous experimental study.

It is also worthwhile to pinpoint here that there have been a large number of experimental studies that have investigated changes, and not inversion, in the ionic current in a PE-grafted nanochannel as a function of the variation of pH. This change in ionic current can be due to the changes in the ionization (and hence charging) of the grafted PE molecule (which, in turn, changes the electric double-layer ion distribution). For example, Ali et al.[66] showed a distinct pH-dependent variation in the ionic current in a conical nanopore functionalized with polyprotic acid chains (with terminated $-PO_3H_2$ groups); a gradual increase in pH (from 3 to 10) led to multistage ionization of the $-PO_3H_2$ groups converting the nanopore from uncharged to highly negatively charged, which, in turn, led to large positive current for positive applied voltage and very weak negative current for negative applied voltage. In another study, Ali et al.[6] demonstrated the pH-dependent alteration in ionic current (and hence rectification) in conical nanopores functionalized separately with lysine and histidine. For both types of nanopores, the nature of ionization of lysine and histidine meant that the nanopore became positively charged (causing large negative current for negative applied voltages) and negatively charged (causing large positive current for positive applied voltages) for small (∼2) and large (∼10−11) pH values, respectively. Other similar works demonstrating pH-dependent changes in ionic current in PE-grafted nanopore include the studies by Ali et al.[67] (here pH-dependent charging of the horseradish peroxidase, used to functionalize the nanopore, triggers a pH-dependent change in ionic current and is used to sense hydrogen peroxide), Yameen et al.[68] (here pH-dependent charging of the phosphate-bearing PE chains, used to functionalize the nanopore, ensured an enhanced negative surface charge density of the nanopore at large pH causing a large positive current with a positive voltage), Yameen et al.[2] (here pH-dependent charging of the zwitterionic PE chains, used to functionalize the nanopore, caused a positive (negative) nanopore surface charge at small (large) pH causing a large negative (positive) current with a negative (positive) applied voltage), and so on. pH-dependent change in ionic current in a PE-grafted nanopore is also possible via a pH-dependent change in the physical configuration of the grafted PE. Xia et al.[69] considered a nanopore grafted with a pH-responsive DNA motor, which attained a single-stranded structure at large pH (∼8.5) and an *i-motif* structure at small pH (∼4.5); as a consequence, the nanopore exhibited an "on" state (where there is large current flow) and an "off" state (where there is a very weak current flow) at large and small pH values. de Groot et al.[1] considered nanopores grafted with pH-responsive poly(methacrylic acid) or PMMA; PMMA became charged and swollen at larger pH, causing a large value of conducted current. Yameen et al.[70] studied ionic transport in cylindrical nanochannels grafted with poly(4-vinylpyridine) brushes; these brushes charged and swelled at smaller pH, thereby significantly enhancing the current conduction. All of these examples discussed here, unlike what we propose in this paper, simply report a pH-dependent *change* in ionic current (where the ionic current is always counterion dominated) and not an inversion of ionic current (where the current becomes co-ion-dominated and changes sign without any sign change of the applied potential).

DOI: 10.1021/acs.jpcb.5b07167
J. Phys. Chem. B XXXX, XXX, XXX−XXX

A straightforward way to experimentally witness our proposed current inversion will be operate in the proposed parameter space (see Figures 3a and 4). This inversion will be signaled by a change in sign of the current despite no change in the sign of the applied voltage in the $I-V$ curve characterizing the PE-grafted nanochannel. In other words, a positive applied potential will lead to a negative current signaling the current inversion. We are not aware of the existence of such an $I-V$ curve for a PE-grafted nanochannel/nanopore; new experiments are needed to obtain such a curve and confirm our theoretical prediction of current inversion.

Practicality of the $\sigma-N$ Phase Diagram. It is important to test the practicality of our predicted $\sigma-N$ phase diagram. (See Figure 2.) Such testing establishes what combination of the $\sigma-N$ values in the hashed zone (i.e., the $\sigma-N$ combinations that ensure that the grafted PE layers form brushes that have height lesser than the nanochannel half height) are practically realizable. For example, Figure 2a shows that for grafted PAA chains $\sigma \approx 10^2$ nm^{-2} and $N \approx 10$ will lead to brush formation that has a height smaller than the nanochannel half height; however, such a value of σ is too high because it leads to an impractical separation distance (between grafted polymers) of $\sigma^{-1/2} \approx 0.1$ nm. On the contrary, $\sigma \approx 10^{-2}$ nm^{-2} (which leads to a separation distance of $\sigma^{-1/2} \approx 10$ nm) and $N \approx 100$ provide a much more practically realizable option; please note that we have identified such a combination for our modeling (see before eq 14). For DNA chains, the hashed zone occupies a much smaller area (see Figure 2b), indicating a much limited combination of $\sigma-N$ values that will ensure the formation of brushes having a height smaller than the nanochannel height. For a finite N ($0 < N < 10$), the corresponding σ value ranges from 10^{-4} to 10^{-2} nm^2, which leads to a separation distance of $\sigma^{-1/2} \approx 10-100$ nm. Given the DNA thickness of more than a nanometer, such a choice of separation distance is pretty reasonable.

Applicability of the Mean Field Approach for the Present Nanoscale Systems. Our mean field approach, which leads to a continuum description of EDL electrostatics and the resulting ion transport, is valid for the present case of channel height of 200 nm (channel half height is $h = 100$ nm). Typically, the atomistic details, beyond the tractability of the continuum calculations, become necessary if the nanochannel dimensions are only a few nanometers or even less. For such dimensions, sizes of the individual ions and the water molecules become comparable to the channel dimensions necessitating the use of atomistic models. Therefore, ionic transport and ionic current have been modeled atomistically for channels/pores dimensions of 3 (α-hemolysin nanopore),[71] 1 (polymeric nanopores),[72] 3 (nanopore in Si_3N_4 membrane),[73] 1−3 (silica nanopore),[74] 1.4 (nanopore in a heterogeneous membrane),[75] 5.42 (carbon nanotube),[76] 2.22 (finite length silicon nanochannel),[77] 3.49 nm (finite length silicon nanochannel),[78] and so on. On the contrary, continuum analyses (involving Poisson−Boltzmann or Poisson-Nernst−Planck equations) have been routinely used to model EDL electroststics and ion transport in nanochannels of dimensions on the order of tens to hundreds of nanometers.[79−88] These continuum models have been successful to quantify several experimental findings associated with the ion and liquid transport in such nanochannels. Some such examples include the quantification of (a) nanochannel (dimensions varying from 70 to 1147 nm) streaming current generation,[89] (b) ionic current rectification in conical nanopores (nanopore dimensions varying from 3 and 3.5 nm (narrower section) to 265 and 340 nm (wider section); continuum theory proposed by Kosińska et al.[90] reproduced the experimental results of Siwy et al.[91,92]), (c) stalling electrophoretic force on a single DNA molecule translocating through a solid-state nanopore (pore diameter ranging from 6 to 90 nm),[93] (d) relative modulation of ionic current as a function of salt concentration in nanopores (nanopore dimension of 10 nm; continuum theory proposed by Kesselheim et al.[94] reproduces the experimental result of Smeets et al.[95]), (e) ion rectification ratio in branching nanochannel array (nanochannel dimensions 40 and 100 nm),[96] (f) electroosmotic mobilities in nanochannels of different half heights (nanochannel dimensions of 27, 54, and 108 nm),[97] (g) current blockage during threading of single DNA in a boron nitride nanopore (nanopore dimension 8−12.3 nm),[98] and many more. From the above examples, we can justify our use of mean-field approach (yielding a continuum description) for modeling EDL electrostatics and ion transport in nanochannels of height 200 nm.

CONCLUSIONS

We have first established a scaling framework to pinpoint the $\sigma-N$ phase space of the grafted PE molecule, which ensures (a) the grafted PE molecules form brush-like configuration, (b) the height of the PE brush is smaller than the nanochannel half height, and (c) the PE electrostatic effects can be decoupled from the PE entropic and excluded volume effects. Second, we have calculated the ionic current for such PE-grafted nanochannels for system parameters that ensure that the nanochannel functions in this decoupled regime. The analysis is based on the mean-field-based model of calculating the PE-charge-induced EDL electrostatics. The most important result in this context is the identification of inversion of ionic current for certain choices of system parameters. This inversion occurs because the ionic current becomes bulk current (and hence "co-ion") dominated, with negligible influence of the EDL current. To the best of our knowledge, there has been no experimental identification of this ionic current inversion phenomenon. Provided one chooses the appropriate parameter space (e.g., appropriate combination of σ, N, PE molecule, pH_∞, pK_a, and n_∞) it will be straightforward to observe this current inversion through the classical current−voltage plot used to characterize the transport properties of PE-grafted nanochannels.[2−4,45−47,67,69] Also, the PE layers will substantially suppress the background electroosmotic transport, thereby ensuring a highly accurate current−voltage response.[13] Given the ubiquitous use of the change in the current−voltage response characteristics of a nanochannel to sense a bioanalyte or fabricate a nanofluidic diode or rectifier, our findings are expected to influence several applications associated with "smart" PE-grafted nanochannels. Of course, there are more rigorous numerical self-consistent-field-theory approaches for probing the electrostatics (and the phenomena resulting from such electrostatics) for PE brushes,[99−102] although only very few studies[99] attempt to capture the behavior of PE brushes with pH-dependent charge density. We expect that this highly nonintuitive result of current inversion, which holds important bearing in operation of functionalized nanochannels, will be scrutinized and tested through these approaches in near future.

AUTHOR INFORMATION

Corresponding Author

*Phone:+1-301-405-6633. E-mail: sidd@umd.edu.

DOI: 10.1021/acs.jpcb.5b07167
J. Phys. Chem. B XXXX, XXX, XXX−XXX

Notes

The authors declare no competing financial interest.

REFERENCES

(1) de Groot, G. W.; Santonicola, M. G.; Sugihara, K.; Zambelli, T.; Reimhult, E.; Vörös, J.; Vancso, G. J. Switching transport through nanopores with pH-responsive polymer brushes for controlled ion permeability. *ACS Appl. Mater. Interfaces* **2013**, *5*, 1400−1407.

(2) Yameen, B.; Ali, M.; Neumann, R.; Ensinger, W.; Knoll, W.; Azzaroni, O. Single conical nanopores displaying ph-tunable rectifying characteristics. Manipulating ionic transport with zwitterionic polymer brushes. *J. Am. Chem. Soc.* **2009**, *131*, 2070−2071.

(3) Ali, M.; Yameen, B.; Cervera, J.; Ramirez, P.; Neumann, R.; Ensinger, W.; Knoll, W.; Azzaroni, O. Layer-by-layer assembly of polyelectrolytes into ionic current rectifying solid-state nanopores: Insights from theory and experiment. *J. Am. Chem. Soc.* **2010**, *132*, 8338−8348.

(4) Ali, M.; Yameen, B.; Neumann, R.; Ensinger, W.; Knoll, W.; Azzaroni, O. Biosensing and supramolecular bioconjugation in single conical polymer nanochannels. Facile incorporation of biorecognition elements into nanoconfined geometries. *J. Am. Chem. Soc.* **2008**, *130*, 16351−16357.

(5) Vilozny, B.; Wollenberg, A. L.; Actis, P.; Hwang, D.; Singaram, B.; Pourmand, N. Carbohydrate-actuated nanofluidic diode: switchable current rectification in a nanopipette. *Nanoscale* **2013**, *5*, 9214−9221.

(6) Ali, M.; Ramirez, P.; Mafe, S.; Neumann, R.; Ensinger, W. A pH-tunable nanofluidic diode with a broad range of rectifying properties. *ACS Nano* **2009**, *3*, 603−608.

(7) Ali, M.; Schiedt, B.; Neumann, R.; Ensinger, W. Biosensing with functionalized single asymmetric polymer nanochannels. *Macromol. Biosci.* **2010**, *10*, 28−32.

(8) Umehara, S.; Karhanek, M.; Davis, R. W.; Pourmand, N. Label-free biosensing with functionalized nanopipette probes. *Proc. Natl. Acad. Sci. U. S. A.* **2009**, *106*, 4611−4616.

(9) Adiga, S.; Brenner, D. W. Stimuli-responsive polymer brushes for flow control through nanopores. *J. Funct. Biomater.* **2012**, *3*, 239−256.

(10) Chanda, S.; Sinha, S.; Das, S. Streaming potential and electroviscous effects in soft nanochannels: Towards designing more efficient nanofluidic electrochemomechanical energy converters. *Soft Matter* **2014**, *10*, 7558−7568.

(11) Das, S. Explicit interrelationship between Donnan and surface potentials and explicit quantification of capacitance of charged soft interfaces withpH-dependent charge density. *Colloids Surf., A* **2014**, *462*, 69−74.

(12) Chen, G.; Das, S. Electrostatics of soft charged interfaces with pH-dependent charge density: Effect of consideration of appropriate hydrogen ion concentration distribution. *RSC Adv.* **2015**, *5*, 4493−4501.

(13) Chen, G.; Das, S. Electroosmotic transport in polyelectrolyte-grafted nanochannels with pH-dependent charge density. *J. Appl. Phys.* **2015**, *117*, 185304(1−9).

(14) Chen, G.; Das, S. Streaming potential and electroviscous effects in soft nanochannels beyond Debye-Hückel linearization. *J. Colloid Interface Sci.* **2015**, *445*, 357−363.

(15) Yeh, L.-H.; Zhang, M.; Qian, S.; Hsu, J.-P.; Tseng, S. Ion concentration polarization in polyelectrolyte-modified nanopores. *J. Phys. Chem. C* **2012**, *116*, 8672−8677.

(16) Milne, Z.; Yeh, L.-H.; Chou, T.-H.; Qian, S. Tunable Donnan potential and electrokinetic flow in a biomimetic gated nanochannel with pH-regulated polyelectrolyte brushes. *J. Phys. Chem. C* **2014**, *118*, 19806−19813.

(17) Cao, Q.; Zuo, C.; Li, L.; Zhang, Y.; Yan, G. Electro-osmotic flow in nanochannels with voltage-controlled polyelectrolyte brushes: Dependence on grafting density and normal electric field. *J. Polym. Sci., Part B: Polym. Phys.* **2012**, *50*, 805−811.

(18) Ouyang, H.; Xia, Z.; Zhe, J. Voltage-controlled flow regulating in nanofluidic channels with charged polymer brushes. *Microfluid. Nanofluid.* **2010**, *9*, 915−922.

(19) Adiga, S.; Brenner, D. W. Toward designing smart nanovalves: Modeling of flow control through nanopores via the helix?coil transition of grafted polypeptide chains. *Macromolecules* **2007**, *40*, 1342−1348.

(20) Zhulina, E. B.; Borisov, O. V. Structure and interaction of weakly charged polyelectrolyte brushes: Self-consistent field theory. *J. Chem. Phys.* **1997**, *107*, 5952−5967.

(21) Zhulina, E. B.; Borisov, O. V. Poisson-Boltzmann theory of pH-sensitive (annealing) polyelectrolyte brush. *Langmuir* **2011**, *27*, 10615−10633.

(22) Tagliazucchi, M.; Azzaroni, O.; Szleifer, I. Responsive polymers end-tethered in solid-state nanochannels: When nanoconfinement really matters. *J. Am. Chem. Soc.* **2010**, *132*, 12404−12411.

(23) Tsori, Y.; Andelman, D.; Joanny, J.-F. Interfacial instability of chargedDend-group polymer brushes. *Eur. Phys. Lett.* **2008**, *82*, 46001(1−6).

(24) Ohshima, H. Theory of electrostatics and electrokinetics of soft particles. *Sci. Technol. Adv. Mater.* **2009**, *10*, 063001(1−13).

(25) Ohshima, H. Electrical phenomena in a suspension of soft particles. *Soft Matter* **2012**, *8*, 3511−3514.

(26) Barbati, A. C.; Kirby, B. J. Soft diffuse interfaces in electrokinetics - theory and experiment for transport in charged diffuse layers. *Soft Matter* **2012**, *8*, 10598−10613.

(27) Ohshima, H. Electrostatic interaction between soft particles. *J. Colloid Interface Sci.* **2008**, *328*, 3−9.

(28) Makino, K.; Ohshima, H. Soft particle analysis of electrokinetics of biological cells and their model systems. *Sci. Technol. Adv. Mater.* **2011**, *12*, 023001(1−13).

(29) Ohshima, H. Electrostatic repulsion between two parallel plates covered with polymer brush layers. *Colloid Polym. Sci.* **1999**, *277*, 535−540.

(30) Ohshima, H. Electrostatic repulsion between two parallel plates covered with polyelectrolyte brush layers. Effects of interdigitation. *Colloid Polym. Sci.* **2014**, *292*, 431−439.

(31) Grosberg, A. Y.; Nguyen, T. T.; Shklovskii, B. I. *Colloquium*: The physics of charge inversion in chemical and biological systems. *Rev. Mod. Phys.* **2002**, *74*, 329−345.

(32) Pittler, J.; Bu, W.; Vaknin, D.; Travesset, A.; McGillivray, D. J.; Lösche, M. Charge inversion at minute electrolyte concentrations. *Phys. Rev. Lett.* **2006**, *97*, 046102(1−4).

(33) Kim, Y. W.; Sung, W. Charge inversion on membranes induced by multivalent-counterion fluctuations. *J. Phys.: Condens. Matter* **2005**, *17*, S2943−S2949.

(34) Besteman, K.; Zevenbergen, M. A. G.; Heering, H. A.; Lemay, S. G. Direct observation of charge inversion by multivalent ions as a universal electrostatic phenomenon. *Phys. Rev. Lett.* **2004**, *93*, 170802(1−4).

(35) Tan, Q.; Zhao, G.; Qiu, Y.; Kan, Y.; Ni, Z.; Chen, Y. Experimental observation of the ion?ion correlation effects on charge inversion and strong adhesion between mica surfaces in aqueous electrolyte solutions. *Langmuir* **2014**, *30*, 10845−10854.

(36) Greberg, H.; Kjellander, R. Charge inversion in electric double layers and effects of different sizes for counterions and coions. *J. Chem. Phys.* **1998**, *108*, 2940−2953.

(37) van der Heyden, F. H. J.; Stein, D.; Besteman, K.; Lemay, S. G.; Dekker, C. Charge inversion at high ionic strength studied by streaming currents. *Phys. Rev. Lett.* **2006**, *96*, 224502(1−4).

(38) Labbez, C.; Jönsson, B.; Skarba, M.; Borkovec, M. Ion-ion correlation and charge reversal at titrating solid interfaces. *Langmuir* **2009**, *25*, 7209−7213.

(39) Hoffmann, J.; Gillespie, D. Ion correlations in nanofluidic channels: Effects of ion size, valence, and concentration on voltage- and pressure-driven currents. *Langmuir* **2013**, *29*, 1303−1317.

(40) Buyukdagli, S.; Blossey, R.; Ala-Nissila, T. Ionic current inversion in pressure-driven polymer translocation through nanopores. *Phys. Rev. Lett.* **2015**, *114*, 088303.

(41) Chakraborty, S.; Das, S. Streaming-field-induced convective transport and its influence on the electroviscous effects in narrow

DOI: 10.1021/acs.jpcb.5b07167
J. Phys. Chem. B XXXX, XXX, XXX−XXX

fluidic confinement beyond the Debye-Hückel limit. *Phys. Rev. E* **2008**, *77*, 037303(1−4).
(42) Das, S.; Chakraborty, S. Influence of streaming potential on the transport and separation of charged spherical solutes in nanochannels subjected to particle-wall interactions. *Langmuir* **2009**, *25*, 9863−9872.
(43) Das, T.; Das, S.; Chakraborty, S. Influences of streaming potential on cross stream migration of flexible polymer molecules in nanochannel flows. *J. Chem. Phys.* **2009**, *130*, 244904(1−12).
(44) Das, S.; Chakraborty, S. Effect of conductivity variations within the electric double layer on the streaming potential estimation in narrow fluidic confinements. *Langmuir* **2010**, *26*, 11589−11596.
(45) Xie, G.; Tian, W.; Wen, L.; Xiao, K.; Zhang, Z.; Liu, Q.; Hou, G.; Li, P.; Tian, Y.; Jiang, L. Chiral recognition of L-tryptophan with beta-cyclodextrin-modified biomimetic single nanochannel. *Chem. Commun.* **2015**, *51*, 3135−3138.
(46) Siwy, Z.; Trofin, L.; Kohli, P.; Baker, L. A.; Trautmann, C.; Martin, C. R. Protein biosensors based on biofunctionalized conical gold nanotubes. *J. Am. Chem. Soc.* **2005**, *127*, 5000−5001.
(47) Ali, M.; Neumann, R.; Ensinger, W. Sequence-specific recognition of DNA oligomer using peptide nucleic acid (PNA)-modified synthetic ion channels: PNA/DNA hybridization in nanoconfined environment. *ACS Nano* **2010**, *4*, 7267−7274.
(48) Alexander, S. Polymer adsorption on small spheres. A scaling approach. *J. Phys. (Paris)* **1977**, *38*, 977−981.
(49) de Gennes, P. G. Scaling theory of polymer adsorption. *J. Phys. (Paris)* **1976**, *37*, 1445−1452.
(50) de Gennes, P. G. Conformations of polymers attached to an interface. *Macromolecules* **1980**, *13*, 1069−1075.
(51) Milner, S. T. Polymer brushes. *Science* **1991**, *251*, 905−914.
(52) Netz, R. R.; Andelman, D. Neutral and charged polymers at interfaces. *Phys. Rep.* **2003**, *380*, 1−95.
(53) Odijk, T. Polyelectrolytes near the rod limit. *J. Polym. Sci., Polym. Phys. Ed.* **1977**, *15*, 477−483.
(54) Odijk, T.; Houwaart, A. C. On the theory of the excluded-volume effect of a polyelectrolyte in a 1−1 electrolyte solution. *J. Polym. Sci., Polym. Phys. Ed.* **1978**, *16*, 627−629.
(55) Skolnick, J.; Fixman, M. Electrostatic persistence length of a wormlike polyelectrolyte. *Macromolecules* **1977**, *10*, 944−948.
(56) Ha, B.-Y.; Thirumalai, D. Electrostatic persistence length of a polyelectrolyte chain. *Macromolecules* **1995**, *28*, 577−581.
(57) Cranford, S. W.; Buehler, M. J. Variation of weak polyelectrolyte persistence length through an electrostatic contour length. *Macromolecules* **2012**, *45*, 8067−8082.
(58) Zhulina, E. B.; Rubinstein, M. Ionic strength dependence of polyelectrolyte brush thickness. *Soft Matter* **2012**, *8*, 9376−9383.
(59) Miquelard-Garnier, G.; Creton, C.; Hourdet, D. Strain induced clustering in polyelectrolyte hydrogels. *Soft Matter* **2008**, *4*, 1011−1023.
(60) Reneker, D. H.; Chun, I. Nanometre diameter fibres of polymer, produced by electrospinning. *Nanotechnology* **1996**, *7*, 216−223.
(61) Baldessari, F.; Santiago, J. G. Electrokinetics in nanochannels Part I. Electric double layer overlap and channel-to-well equilibrium. *J. Colloid Interface Sci.* **2008**, *325*, 526−538.
(62) Das, S.; Guha, A.; Mitra, S. K. Exploring new scaling regimes for streaming potential andelectroviscous effects in a nanocapillary with overlapping Electric Double Layers. *Anal. Chim. Acta* **2013**, *804*, 159−166.
(63) Das, S.; Chanda, S.; Eijkel, J. C. T.; Tas, N. R.; Chakraborty, S.; Mitra, S. K. Filling of charged cylindrical capillaries. *Phys. Rev. E* **2014**, *90*, 043011(1−11).
(64) Das, S.; Dubsky, P.; van den Berg, A.; Eijkel, J. C. T. Concentration polarization in translocation of DNA through nanopores and nanochannels. *Phys. Rev. Lett.* **2012**, *108*, 138101(1−5).
(65) He, Y.; Gillespie, D.; Boda, D.; Vlassiouk, I.; Eisenberg, R. S.; Siwy, Z. S. Tuning transport properties of nanofluidic devices with local charge inversion. *J. Am. Chem. Soc.* **2009**, *131*, 5194−5202.
(66) Ali, M.; Mafe, S.; Ramirez, P.; Neumann, R.; Ensinger, W. Logic gates using nanofluidic diodes based on conical nanopores functionalized with polyprotic acid chains. *Langmuir* **2009**, *25*, 11993−11997.
(67) Ali, M.; Tahir, M. N.; Siwy, Z.; Neumann, R.; Tremel, W.; Ensinger, W. Hydrogen peroxide sensing with horseradish peroxidase-modified polymer single conical nanochannels. *Anal. Chem.* **2011**, *83*, 1673−1680.
(68) Yameen, B.; Ali, M.; Neumann, R.; Ensinger, W.; Knoll, W.; Azzaroni, O. Proton-regulated rectified ionic transport through solid-state conical nanopores modified with phosphate-bearing polymer brushes. *Chem. Commun.* **2010**, *46*, 1908−1910.
(69) Xia, F.; Guo, W.; Mao, Y.; Hou, X.; Xue, J.; Xia, H.; Wang, L.; Song, Y.; Ji, H.; Ouyang, Q.; Wang, Y.; Jiang, L. Gating of single synthetic nanopores by proton-driven DNA molecular motors. *J. Am. Chem. Soc.* **2008**, *130*, 8345−8350.
(70) Yameen, B.; Ali, M.; Neumann, R.; Ensinger, W.; Knoll, W.; Azzaroni, O. Synthetic proton-gated ion channels via single solid-state nanochannels modified with responsive polymer brushes. *Nano Lett.* **2009**, *9*, 2788−2793.
(71) Aksimentiev, A.; Schulten, K. Imaging α-hemolysin with molecular dynamics: Ionic conductance, osmotic permeability, and the electrostatic potential map. *Biophys. J.* **2005**, *88*, 3745−3761.
(72) Cruz-Chu, E. R.; Ritz, T.; Siwy, Z. Z.; Schulten, K. Molecular control of ionic conduction in polymer nanopores. *Faraday Discuss.* **2009**, *143*, 47−93.
(73) Aksimentiev, A. Deciphering ionic current signatures of DNA transport through a nanopore. *Nanoscale* **2010**, *2*, 468−483.
(74) Cruz-Chu, E. R.; Aksimentiev, A.; Schulten, K. Ionic current rectification through silica nanopores. *J. Phys. Chem. C* **2009**, *113*, 1850−1862.
(75) Qiao, R.; Georgiadis, J. G.; Aluru, N. R. Differential ion transport induced electroosmosis and internal recirculation in heterogeneous osmosis membranes. *Nano Lett.* **2006**, *6*, 995−999.
(76) Qiao, R.; Aluru, N. R. Atypical dependence of electroosmotic transport on surface charge in a single-wall carbon nanotube. *Nano Lett.* **2003**, *3*, 1013−1017.
(77) Qiao, R.; Aluru, N. R. Ion concentrations and velocity profiles in nanochannel electroosmotic flows. *J. Chem. Phys.* **2003**, *118*, 4692−4701.
(78) Qiao, R.; Aluru, N. R. Surface-charge-induced asymmetric electrokinetic transport in confined silicon nanochannels. *Appl. Phys. Lett.* **2005**, *86*, 143105(1−3).
(79) Movahed, S.; Li, D. Electrokinetic transport through nanochannels. *Electrophoresis* **2011**, *32*, 1259−1267.
(80) Movahed, S.; Li, D. Electrokinetic transport through the nanopores in cell membrane during electroporation. *J. Colloid Interface Sci.* **2012**, *369*, 442−452.
(81) Zhang, M.; Ai, Y.; Sharma, A.; Joo, S. W.; Kim, D. S.; Qian, S. Electrokinetic particle translocation through a nanopore containing a floating electrode. *Electrophoresis* **2011**, *32*, 1864−1874.
(82) Ai, Y.; Qian, S. Direct numerical simulation of electrokinetic translocation of a cylindrical particle through a nanopore using a PoissonÐBoltzmann approach. *Electrophoresis* **2011**, *32*, 996−1005.
(83) Ai, Y.; Qian, S. Electrokinetic particle translocation through a nanopore. *Phys. Chem. Chem. Phys.* **2011**, *13*, 4060−4071.
(84) Qian, S.; Das, B.; Luo, X. Diffusioosmotic flows in slit nanochannels. *J. Colloid Interface Sci.* **2007**, *315*, 721−30.
(85) Pennathur, S.; Santiago, J. G. Electrokinetic transport in nanochannels. 1. Theory. *Anal. Chem.* **2005**, *77*, 6772−6781.
(86) Yuan, Z.; Garcia, A. L.; Lopez, G. P.; Petsev, D. N. Electrokinetic transport and separations in fluidic nanochannels. *Electrophoresis* **2007**, *28*, 595−610.
(87) Swaminathan, V. N.; Gibson, L. R., II; Pinti, M.; Prakash, S.; Bohn, P. W.; Shannon, M. A. Ionic transport in nanocapillary membrane systems. *J. Nanopart. Res.* **2012**, *14*, 951(1−15).
(88) Guan, W.; Li, S. X.; Reed, M. A. Voltage gated ion and molecule transport in engineered nanochannels: theory, fabrication and applications. *Nanotechnology* **2014**, *25*, 122001(1−19).
(89) van der Heyden, F. H. J.; Stein, D.; Dekker, C. Streaming currents in a single nanofluidic channel. *Phys. Rev. Lett.* **2005**, *95*, 116104(1−4).

DOI: 10.1021/acs.jpcb.5b07167
J. Phys. Chem. B XXXX, XXX, XXX−XXX

(90) Kosińska, I. D.; Goychuk, I.; Kostur, M.; Schmid, G. Rectification in synthetic conical nanopores: A one-dimensional Poisson-Nernst-Planck model. *Phys. Rev. E* **2008**, *77*, 198103(1−4).
(91) Siwy, Z.; Fuliński, A. Fabrication of a synthetic nanopore ion pump. *Phys. Rev. Lett.* **2002**, *89*, 198103(1−4).
(92) Siwy, Z. S. Ion-current rectification in nanopores and nanotubes with broken symmetry. *Adv. Funct. Mater.* **2006**, *16*, 735−746.
(93) van Dorp, S.; Keyser, U. F.; Dekker, N. H.; Dekker, C.; Lemay, S. G. Origin of the electrophoretic force on DNA in solid-state nanopores. *Nat. Phys.* **2009**, *5*, 347−351.
(94) Kesselheim, S.; Müller, W.; Holm, C. Origin of current blockades in nanopore translocation experiments. *Phys. Rev. Lett.* **2014**, *112*, 018101(1−4).
(95) Smeets, R. M. M.; Keyser, U. F.; Krapf, D.; Wu, M.-Y.; Dekker, N. H.; Dekker, C. Salt dependence of ion transport and DNA translocation through solid-state nanopores. *Nano Lett.* **2006**, *6*, 89−95.
(96) Li, C.-Y.; Wu, Z.-Q.; Yuan, C.-G.; Wang, K.; Xia, X.-H. Propagation of concentration polarization affecting ions transport in branching nanochannel array. *Anal. Chem.* **2015**, *87*, 8194−8202.
(97) Haywood, D. G.; Harms, Z. D.; Jacobson, S. C. Electroosmotic flow in nanofluidic channels. *Anal. Chem.* **2014**, *86*, 11174−11180.
(98) Liu, S.; Lu, B.; Zhao, Q.; Li, J.; Gao, T.; Chen, Y.; Zhang, Y.; Liu, Z.; Fan, Z.; Yang, F.; You, L.; Yu, D. Boron Nitride nanopores: Highly sensitive DNA single-molecule detectors. *Adv. Mater.* **2013**, *25*, 4549−4554.
(99) Witte, K. N.; Kim, S.; Won, Y.-Y. Self-consistent field theory study of the effect of grafting density on the height of a weak polyelectrolyte brush. *J. Phys. Chem. B* **2009**, *113*, 11076−11084.
(100) Qu, L.-J.; Jin, X.; Liao, Q. Numerical self-consistent field theory of cylindrical polyelectrolyte brushes. *Macromol. Theory Simul.* **2009**, *18*, 162−170.
(101) Wang, L.; Jiang, T.; Lin, J. Self-assembly of graft copolymers in backbone-selective solvents: a route toward stable hierarchical vesicles. *RSC Adv.* **2013**, *3*, 19481−19491.
(102) Quan, G.; Wang, M.; Tong, C. A numerical study of spherical polyelectrolyte brushes by the self-consistent field theory. *Polymer* **2014**, *55*, 6604−6613.

DOI: 10.1021/acs.jpcb.5b07167
J. Phys. Chem. B XXXX, XXX, XXX−XXX